

Published in final edited form as:

J Am Chem Soc. 2011 November 9; 133(44): 17602–17605. doi:10.1021/ja207882h.

Rapid C-H Bond Activation by a Monocopper(III)-Hydroxide Complex

Patrick J. Donoghue¹, Jacqui Tehranchi¹, Christopher J. Cramer¹, Ritimukta Sarangi², Edward I. Solomon^{2,3}, and William B. Tolman^{1,*}

¹Department of Chemistry, Center for Metals in Biocatalysis, and Supercomputer Institute, University of Minnesota, 207 Pleasant St. SE, Minneapolis, MN 55455

²Stanford Synchrotron Radiation Lightsource, SLAC National Accelerator Laboratory, Menlo Park, CA 94025

³Department of Chemistry, Stanford University, Stanford, CA 94305

Abstract

One electron oxidation of the tetragonal Cu(II) complex [Bu₄N][LCuOH] at –80 °C generated the reactive intermediate LCuOH, which was shown to be a Cu(III) complex on the basis of spectroscopy and theory (L = *N,N'*-bis(2,6-diisopropylphenyl)-2,6-pyridinedicarboxamide). The complex LCuOH reacts with dihydroanthracene to yield anthracene and the Cu(II) complex LCu(OH₂). Kinetic studies showed that the reaction occurs via H-atom abstraction via a second-order rate law at high rates (cf. $k = 1.1(1) \text{ M}^{-1}\text{s}^{-1}$ at –80 °C, $\Delta H^\ddagger = 5.4(2) \text{ kcal mol}^{-1}$, $\Delta S^\ddagger = -30(2) \text{ eu}$) and with very large kinetic isotope effects (cf. $k_{\text{H}}/k_{\text{D}} = 44$ at –70 °C). The findings suggest that a Cu(III)-OH moiety is a viable reactant in oxidation catalysis.

Copper-oxygen species are implicated as intermediates in a wide range of oxidation reactions promoted by metalloenzymes,¹ synthetic complexes,^{2,3} and materials.⁴ Understanding the structures, properties, and reactivities of such species is critical for obtaining mechanistic insights into oxidation catalysis and for developing new, selective catalytic reagents and processes. Efforts to isolate and characterize reactive copper-oxygen intermediates through studies of copper-containing enzymes and synthetic model complexes have led to the identification of several core motifs,⁵ exemplified by those shown in Chart 1. Complexes comprising cores **A–E** have been well-defined, and as a result have often been considered as viable oxidants in various catalytic reactions.⁶ The monocopper-oxo/oxyl core (**F**) has also been discussed⁷ as a candidate capable of attacking hydrocarbon substrates (cf. by peptidylglycine α -hydroxylating monooxygenase⁸) but examples of such species have only been characterized in the gas phase⁹ and through theoretical calculations.^{8,10} We report herein the preparation and characterization by spectroscopy and theory of a new type of copper-oxygen intermediate containing a hydroxo-copper(III) core (**G**), which formally may be considered as a protonated version of **F**.¹¹ The complex comprising **G** rapidly abstracts hydrogen atoms from the C-H bonds of dihydroanthracene, thus providing key precedent for the possible involvement of **G** in oxidation catalysis.

Corresponding Author wtolman@umn.edu.

ASSOCIATED CONTENT

Supporting Information. Experimental details, including characterization data, spectra, X-ray structure drawings, kinetic plots and tables, and calculation protocols and results (PDF) and CIFs. This material is available free of charge via the Internet at <http://pubs.acs.org>.

As starting material we used the tetragonal copper(II) complex $\text{LCu}(\text{CH}_3\text{CN})$ (**1**, $L = N,N'$ -bis(2,6-diisopropylphenyl)-2,6-pyridinedicarboxamide, Figure 1), for which we report a new X-ray crystal structure (Figure S1). Treatment of **1** suspended in Et_2O or dissolved in THF with a solution of Bu_4NX ($X = \text{Cl}$ or OH) in MeOH yielded deep blue or green $[\text{Bu}_4\text{N}][\text{LCuX}]$ ($[\text{Bu}_4\text{N}][\mathbf{2}]$ or $[\text{Bu}_4\text{N}][\mathbf{3}]$), respectively. Both products were isolated as solids and characterized by UV-vis, FTIR, and EPR spectroscopy, and CHN analysis.¹² Notable data include a sharp $\nu(\text{OH})$ at 3628 cm^{-1} in the FTIR spectrum (nujol) of $[\text{Bu}_4\text{N}][\mathbf{3}]$ and essentially axial EPR signals for both complexes consistent with tetragonal Cu(II) species (Figures S2–S3 and Table S1 in the Supporting Information). Crystals of both complexes suitable for characterization by X-ray diffraction were obtained by metathesis with PPNCl (Figures 1 and S4, Table 1). While the structure of $[\text{PPN}][\mathbf{2}]$ is straightforward, in $[\text{PPN}][\mathbf{3}]$ the longer than expected Cu–O distance of $1.947(2)\text{ \AA}$ ¹³ led us to suspect that the crystals were a compositionally disordered¹⁴ mixture of the chloride and hydroxide complexes, with the chloride ligand having been derived from displacement of hydroxide by the added PPNCl. Consistent with this notion, the UV-vis spectral features for $[\text{Bu}_4\text{N}][\mathbf{3}]$ in THF cleanly converted to those for $[\text{Bu}_4\text{N}][\mathbf{2}]$ upon addition of Bu_4NCl (1 equiv. from titration experiments; Figure S5). In addition, comparison of UV-vis spectra of crystals of $[\text{PPN}][\mathbf{3}]$ (3 batches) to those of pure $[\text{Bu}_4\text{N}][\mathbf{2}]$ and $[\text{Bu}_4\text{N}][\mathbf{3}]$ indicated chloride contamination levels of 22–28%. Finally, DFT (*mPW*) calculations were performed for $\mathbf{2}^-$ and $\mathbf{3}^-$ that yielded minimum energy structures with Cu–N bond distances somewhat longer than those measured by X-ray crystallography (Table 1), as is common for *mPW* calculations with bulky ligands.¹⁵ However, a significantly shorter Cu–OH distance was calculated for $\mathbf{3}^-$ (1.863 \AA) than was observed in the X-ray crystal structure ($1.9465(19)\text{ \AA}$). EXAFS data collected for $[\text{Bu}_4\text{N}][\mathbf{3}]$ (powder, not exposed to PPNCl) were best fit with 4N/O donors¹⁶ and average metal–ligand distances of 1.95 \AA (Figures S6 and S7), slightly shorter than those determined by X-ray crystallography and *mPW* (Table 1). The EXAFS data collected for $[\text{Bu}_4\text{N}][\mathbf{2}]$ were best fit with 3 N/O donors averaging 1.98 \AA and one Cl donor at 2.21 \AA , which is also in good agreement with the X-ray crystal structure and *mPW* calculations. Taken together, the data support the hypothesis of a compositionally disordered X-ray crystal structure for $[\text{PPN}][\mathbf{3}]$ with a Cu–O distance that is overestimated by $\sim 0.1\text{ \AA}$.

The tetragonal Cu(II) complex $[\text{Bu}_4\text{N}][\mathbf{3}]$ exhibits a pseudoreversible oxidation in acetone solution ($0.1\text{ M Bu}_4\text{NPF}_6$) at room temperature with $E_{1/2}(\mathbf{3}^-) = -0.076\text{ V vs. Fc}^+/\text{Fc}$ (Figure S11). Chemical oxidation of $[\text{Bu}_4\text{N}][\mathbf{3}]$ in acetone was performed using Fc^+PF_6^- at $-80\text{ }^\circ\text{C}$,¹⁷ which provided a deeply colored purple solution characterized by an intense low energy electronic absorption feature with $\lambda_{\text{max}}(\epsilon) = 540\text{ nm} (\sim 12400\text{ M}^{-1}\text{ cm}^{-1})$ (Figure 2). The solutions were EPR silent. The absorption features decayed within minutes upon warming to $-60\text{ }^\circ\text{C}$. Titration experiments monitored by UV-vis spectroscopy (Figure S12) showed that the oxidation reaction required 1 equivalent of oxidant to reach completion. Reduction of this species with 1 equivalent of decamethylferrocene (Fc^*) to the chilled solution yielded UV-vis features consistent with **3** and Fc^{*+} (Figures S13). These data are consistent with a reversible 1-electron process that generates LCuOH (**4**, Figure 1).

Lacking crystals suitable for X-ray crystallography, we turned to DFT calculations and X-ray absorption spectroscopy to further evaluate the nature of **4**. The one electron oxidation of $\mathbf{3}^-$ could conceivably result in (a) a metal based oxidation to yield a Cu(III) species, or (b) a ligand-based oxidation to yield a Cu(II)-ligand radical. A Cu(III) species should be a singlet whereas a Cu(II)-ligand radical could either be a triplet or an open-shell singlet. Starting from optimized *mPW* structures of $\mathbf{3}^-$, a closed shell singlet structure for **4** was located easily. This oxidized singlet maintained the square-planar geometry and symmetry elements identified in its Cu(II) precursor (C_s). Consistent with the singlet Cu(III) formulation, and in agreement with EXAFS results (see below), upon oxidation of $\mathbf{3}^-$ to **4** the copper–ligand bonds contract; the average Cu–N bond shortens by 0.08 \AA and the Cu–N/O bond average

shortened by 0.09 Å (Table 2). Finally, the results of gas phase time dependent DFT (TD B98) calculations for the singlet of **4** match well with the experimentally observed UV-vis features (Figure S14). Thus, the singlet wavefunction for **4** was calculated to have a single transition at 589 nm (2.10 eV), within 0.2 eV of the observed transition at 540 nm (2.30 eV). The dominant one-electron excitation in this transition, with a weight of about 67%, is from an orbital with largely ligand (L) π character to one largely comprised of the Cu $d_{x^2-y^2}$ (Figure S15). In sum, calculations support a singlet Cu(III) formulation for **4**.

Consistent with this conclusion, structures corresponding to a ligand based oxidation were more difficult to locate by *m*PW. Thus, attempts to identify an open-shell singlet via a broken-symmetry formalism for **4** converged to closed-shell singlet solutions. A triplet structure can be located, but is energetically disfavored relative to the closed-shell singlet by 19.0 kcal/mol. Metal-ligand bond distances calculated for the triplet also are relatively unchanged relative to those calculated for the precursor **3**⁻, in contrast to the EXAFS results (see below). Thus, the triplet **4** actually has a slightly longer average Cu-N/O bond length than the starting complex **3**⁻ (2.01 Å vs 1.99 Å). Finally, TD B98 results for the triplet included several transitions in the near-IR range that were not observed experimentally.

Cu K-edge XAS data provide direct experimental evidence for the Cu(III) formulation of **4**. As shown in Figure 3, the Cu K pre-edge energy position of **4** is shifted ~1.7 eV to higher energy relative to pre-edge of the Cu(II) complex [Bu₄N][**3**], indicating one electron metal based oxidation with an associated increase in ligand field strength of the Cu center. A shift in the rising edge by ~1.1 eV is also observed on going from [Bu₄N][**3**] to **4** reflecting the increase in the effective nuclear charge on Cu in **4**.¹⁸ The EXAFS data (Figures S6 and S8 and Table S3) provide further confirmation of the Cu(III) nature of **4**. Fits to the data show an ~0.1 Å shortening of the first shell Cu-O/N bond distances in **4** (4 Cu-N/O at 1.86 Å) relative to [Bu₄N][**3**] (4 Cu-N/O at 1.95 Å), typical for oxidation of a Cu(II) to a Cu(III) complex.

Inspired by reports of C-H bond activation by Mn(III), Mn(IV), and Fe(III) hydroxide complexes,¹⁹ we examined the reactivity of **4** with dihydroanthracene (DHA), a commonly studied substrate useful for comparison purposes. The UV-vis features of **4** smoothly decayed upon introduction of 0.5 equiv DHA to acetone solutions at low temperature, concomitant with the growth of bands due to the formation of anthracene (85% yield by GC/MS). The final inorganic product was determined to be the Cu(II) complex LCu(OH₂) (**5**, Figure 1) on the basis of comparison of the UV-vis spectrum to that of independently synthesized material, which was fully characterized, including by X-ray crystallography (Figure S16). The UV-vis features of **4** decayed according to pseudo-first-order kinetics when the reaction was performed with excess DHA (10–40 equiv), and a plot of k_{obs} vs. [DHA] was linear with an intercept that corresponded to the self decay rate (Figures S17 and S18). These data indicate an overall second-order rate law $-d[\mathbf{4}]/dt = k[\mathbf{4}][\text{DHA}]$. A very large kinetic isotope effect ($k_{\text{H}}/k_{\text{D}}$) of 44 at -70 °C was observed when the reaction was performed with DHA-*d*₄, and the temperature dependence of this effect was evaluated by an Eyring analysis (Figure 4, Table S4); $\Delta H^{\ddagger}_{\text{H}} = 5.4(2)$ kcal mol⁻¹, $\Delta S^{\ddagger}_{\text{H}} = -30(2)$ eu, $\Delta H^{\ddagger}_{\text{D}} = 6.2(3)$ kcal mol⁻¹, $\Delta S^{\ddagger}_{\text{D}} = -34(3)$ eu. Based on these parameters, the KIE was calculated to be 29 at 20 °C, well beyond the semiclassical limit. Finally, we note that **4** reacted essentially instantaneously at -80 °C with 2,4,6-tri-*tert*-butylphenol to yield the phenoxy radical (UV-vis, EPR). Together, the reactivity and kinetic data support a mechanism for oxidation of DHA to anthracene that involves rate-determining H-atom abstraction by the Cu(III)-OH moiety, with a tunneling contribution being a reasonable rationale for the larger than semiclassically predicted $k_{\text{H}}/k_{\text{D}}$ values.

The second-order rate constants for reactions of selected relevant Cu(III) or metal-oxo or –hydroxo complexes with DHA at $-80\text{ }^{\circ}\text{C}$ are compared to that of **4** in Figure 5.^{20–26} The rate of H-atom abstraction from DHA by LCuOH is significantly faster than most other nonheme iron (b,c,g), manganese (d–f), and copper (a) reagents and is comparable to a recently reported high-spin Fe(III)Fe(IV)-oxo complex (h). While not as intrinsically reactive as the (P⁺)Fe(IV)=O intermediate (compound I) in cytochrome P450,²⁷ the high rate for DHA oxidation by **4** is nonetheless extraordinary in the context of known oxidizing capabilities of copper-oxygen species.^{5,7,28} While further work is necessary to understand the basis for this reactivity, we speculate that high basicity of the hydroxide group is a key factor in view of the fact that the potential for **3**⁻/**4** couple is modest (-0.076 V vs. Fc^+/Fc).²⁹ Similar arguments have been advanced to rationalize observed rates of H-atom transfer by Mn(V)-oxo³⁰ and Fe(IV)-imido³¹ complexes, as well as cuprous oxide surfaces.³² The relatively minor structural differences (overall geometry, metal-ligand bond distances) between **4** and **5** may also result in a small reorganization energy that could contribute to a high reaction rate.³³

In summary, we have prepared a new type of copper-oxygen intermediate and shown through theory and experiment that it is best described as a singlet Cu(III)-OH complex. High rates of H-atom abstraction from phenols and DHA by this complex were observed, indicating that such a species should be considered as a viable intermediate in catalytic oxidation reactions.

Supplementary Material

Refer to Web version on PubMed Central for supplementary material.

Acknowledgments

This research was supported by the NIH (grants R37-GM47365 to W. B. T.; DK-31450 to E. I. S.) and the NSF (CHE-0952054 to CJC). SSRL operations are funded by the Department of Energy, Office of Basic Energy Sciences. The SSRL Structural Molecular Biology program is supported by the National Institutes of Health, National Center for Research Resources, Biomedical Technology Program, and the Department of Energy, Office of Biological and Environmental Research. This publication was made possible by Award P41 RR001209 from the National Center for Research Resources (NCRR), a component of the National Institutes of Health (NIH).

REFERENCES

1. Klinman JP. *Chem. Rev.* 1996; 96:2541–2561. [PubMed: 11848836] Solomon EI, Sundaram UM, Machonkin TE. *Chem. Rev.* 1996; 96:2563–2605. [PubMed: 11848837]
2. Díaz-Requejo MM, Pérez PJ. *Chem. Rev.* 2008; 108:3379–3394. [PubMed: 18698739]
3. Que L Jr, Tolman WB. *Nature.* 2008; 455:333–340. [PubMed: 18800132]
4. Woertink JS, Smeets PJ, Groothaert MH, Vance MA, Sels BF, Schoonheydt RA, Solomon EI. *Proc. Natl. Acad. Sci. USA.* 2009; 106:18908–18913. [PubMed: 19864626]
5. Lewis EA, Tolman WB. *Chem. Rev.* 2004; 104:1047–1076. [PubMed: 14871149] Mirica LM, Ottenwaelder X, Stack TDP. *Chem. Rev.* 2004; 104:1013–1045. [PubMed: 14871148] Hatcher L, Karlin KD. *J. Biol. Inorg. Chem.* 2004; 9:669–683. [PubMed: 15311336] Itoh S. *Curr. Opin. Chem. Biol.* 2006; 10:115–122. [PubMed: 16504568]
6. For example, see: Itoh S, Fukuzumi S. *Acc. Chem. Res.* 2007; 40:592–600. [PubMed: 17461541]
7. Himes RA, Karlin KD. *Curr. Opin. Chem. Biol.* 2009; 13:119–131. and references cited therein. [PubMed: 19286415] Hong S, Gupta AK, Tolman WB. *Inorg. Chem.* 2009; 48:6323–6325. [PubMed: 19425587]
8. Chen P, Solomon EI. *J. Am. Chem. Soc.* 2004; 126:4991–5000. [PubMed: 15080705] Evans JP, Ahn K, Klinman JP. *J. Biol. Chem.* 2003; 278:49691–49698. [PubMed: 12966104] Yoshizawa K, Kihara N, Kamachi T, Shiota Y. *Inorg. Chem.* 2006; 45:3034–3041. [PubMed: 16562959] Crespo

- A, Marti MA, Roitberg AE, Amzel LM, Estrin DA. *J. Am. Chem. Soc.* 2006; 128:12817–12828. [PubMed: 17002377]
9. Schröder D, Holthausen MC, Schwarz H. *J. Phys. Chem. B.* 2004; 108:14407–14416. Dietl N, van der Linde C, Schlangen M, Beyer MK, Schwarz H. *Angew. Chem. Int. Ed.* 2011; 50:4966–4969.
 10. Yoshihide N, Kimihiko H, Tetsuya T. *J. Chem. Phys.* 2001; 114:7935–7940. Decker A, Solomon EI. *Curr. Opin. Chem. Biol.* 2005; 9:152–163. [PubMed: 15811799] Gherman BF, Heppner DE, Tolman WB, Cramer CJ. *J. Biol. Inorg. Chem.* 2006; 11:197–205. [PubMed: 16344970] Huber SM, Ertem MZ, Aquilante F, Gagliardi L, Tolman WB, Cramer CJ. *Chem. Eur. J.* 2009; 15:4886–4895. Gherman BF, Tolman WB, Cramer CJ. *J. Comp. Chem.* 2006; 27:1950–1961. [PubMed: 17019721]
 11. Protonation of a species with core **F** to yield a compound with core **G** has been postulated: Reinaud O, Capdevielle P, Maumy M. *J. Chem. Soc., Chem. Commun.* 1990:566–568.
 12. See the supporting information.
 13. Some reported Cu-OH bond distances in terminal monocopperhydroxide complexes: 1.878(2) Å Berreau LM, Mahapatra S, Halfen JA, Young VG Jr, Tolman WB. *Inorg. Chem.* 1996; 35:6339–6342. 1.875(2) Å. Lee SC, Holm RH. *J. Am. Chem. Soc.* 1993; 115:11789–11198.
 14. Parkin G. *Chem. Rev.* 1993; 93:887–911.
 15. Cramer, CJ. "Essentials of Computational Chemistry: Theories and Models". 2nd ed.. New York: Wiley & Sons; 2004. p. 291
 16. Large Debye-Waller factors for this fit are consistent with a spread of Cu-N/O distances, consistent with the X-ray data and DFT calculations.
 17. XAS samples were prepared using (p-tolyl)₃N⁺PF₆⁻.
 18. DuBois JL, Mukherjee P, Stack TDP, Hedman B, Solomon EI, Hodgson KO. *J. Am. Chem. Soc.* 2000; 122:5775–5787.
 19. Shi S, Wang Y, Xu A, Wang H, Zhu D, Roy SB, Jackson TA, Busch DH, Yin G. *Angew. Chem. Int. Ed.* 2011; 50:7321–7324. and references cited therein.
 20. Lockwood MA, Blubaugh TJ, Collier AM, Lovell S, Mayer JM. *Angew. Chem. Int. Ed.* 1999; 38:225–227.
 21. Roth JP, Mayer JM. *Inorg. Chem.* 1999; 38:2760–2761. [PubMed: 11671018]
 22. Goldsmith CR, Stack TDP. *Inorg. Chem.* 2006; 45:6048–6055. [PubMed: 16842013]
 23. Parsell T, Yang M, Borovik A. *J. Am. Chem. Soc.* 2009; 131:2762–2763. [PubMed: 19196005]
 24. Gardner KA, Kuehnert LL, Mayer JM. *Inorg. Chem.* 1997; 36:2069–2078. [PubMed: 11669825]
 25. Goldsmith CR, Cole AP, Stack TDP. *J. Am. Chem. Soc.* 2005; 127:9904–9912. [PubMed: 15998097]
 26. Xue G, De Hont R, Münck E, Que L Jr. *Nature Chemistry.* 2010; 2:400–405.
 27. Rittle J, Green MT. *Science.* 2010; 330:933–937. [PubMed: 21071661]
 28. Itoh S. *Curr. Opin. Chem. Biol.* 2006; 10:115–122. [PubMed: 16504568]
 29. Green MT. *Curr. Opin. Chem. Biol.* 2009; 13:84–88. [PubMed: 19345605]
 30. Prokop KA, de Visser SP, Goldberg DP. *Angew. Chem. Int. Ed.* 2010; 49:5091–5095.
 31. Nieto I, Ding F, Bontchev RP, Wang H, Smith JM. *J. Am. Chem. Soc.* 2008; 130:2716–2717. [PubMed: 18266366]
 32. Reitz JB, Solomon EI. *J. Am. Chem. Soc.* 1998; 120:11467–11478.
 33. Mayer JM. *Acc. Chem. Res.* 2011; 44:36–46. [PubMed: 20977224]

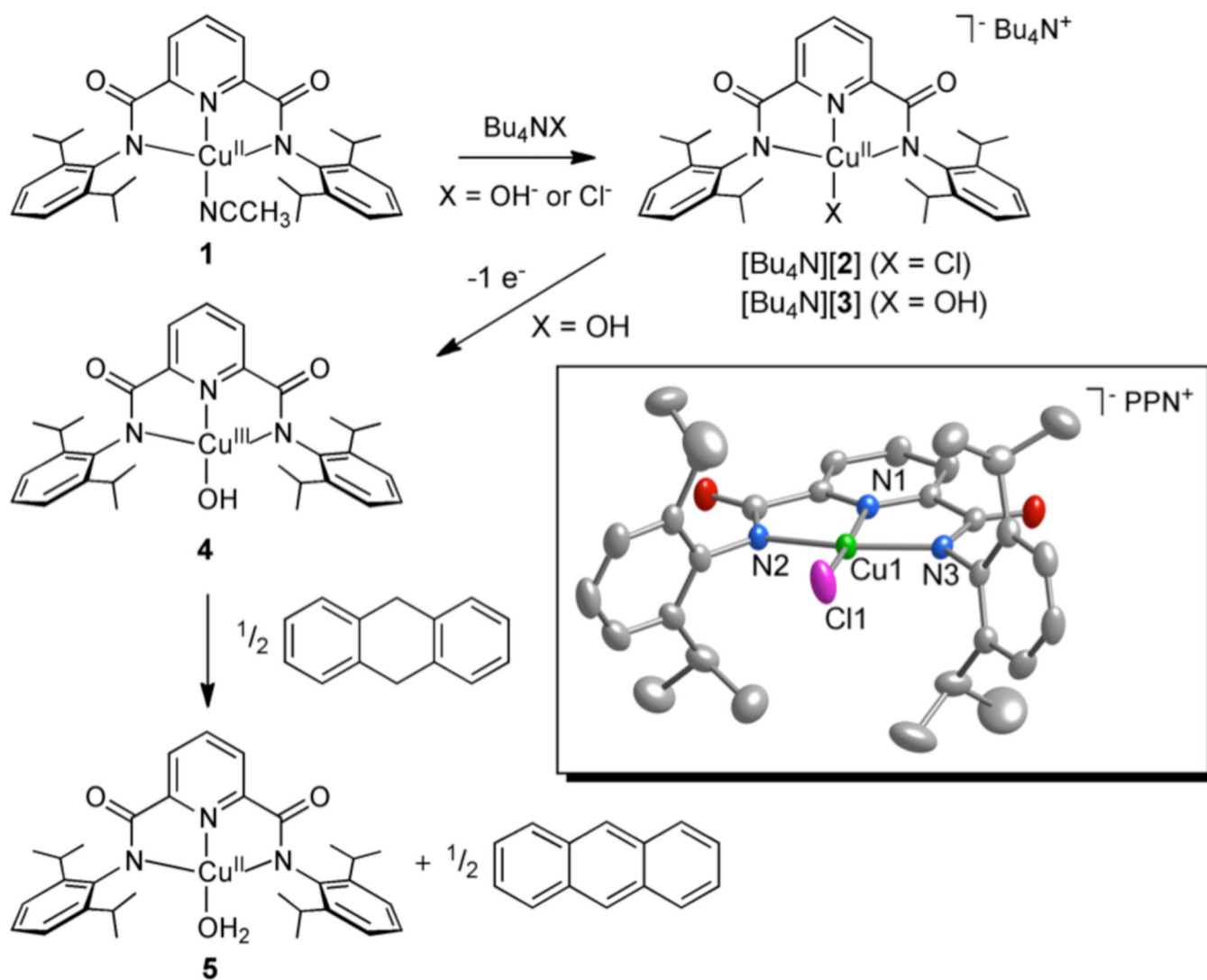


Figure 1. Complexes and reactions studied in this work, with a representation of the anionic portion of the X-ray crystal structure of [PPN][2] shown in the box as 50% thermal ellipsoids (H atoms omitted for clarity).

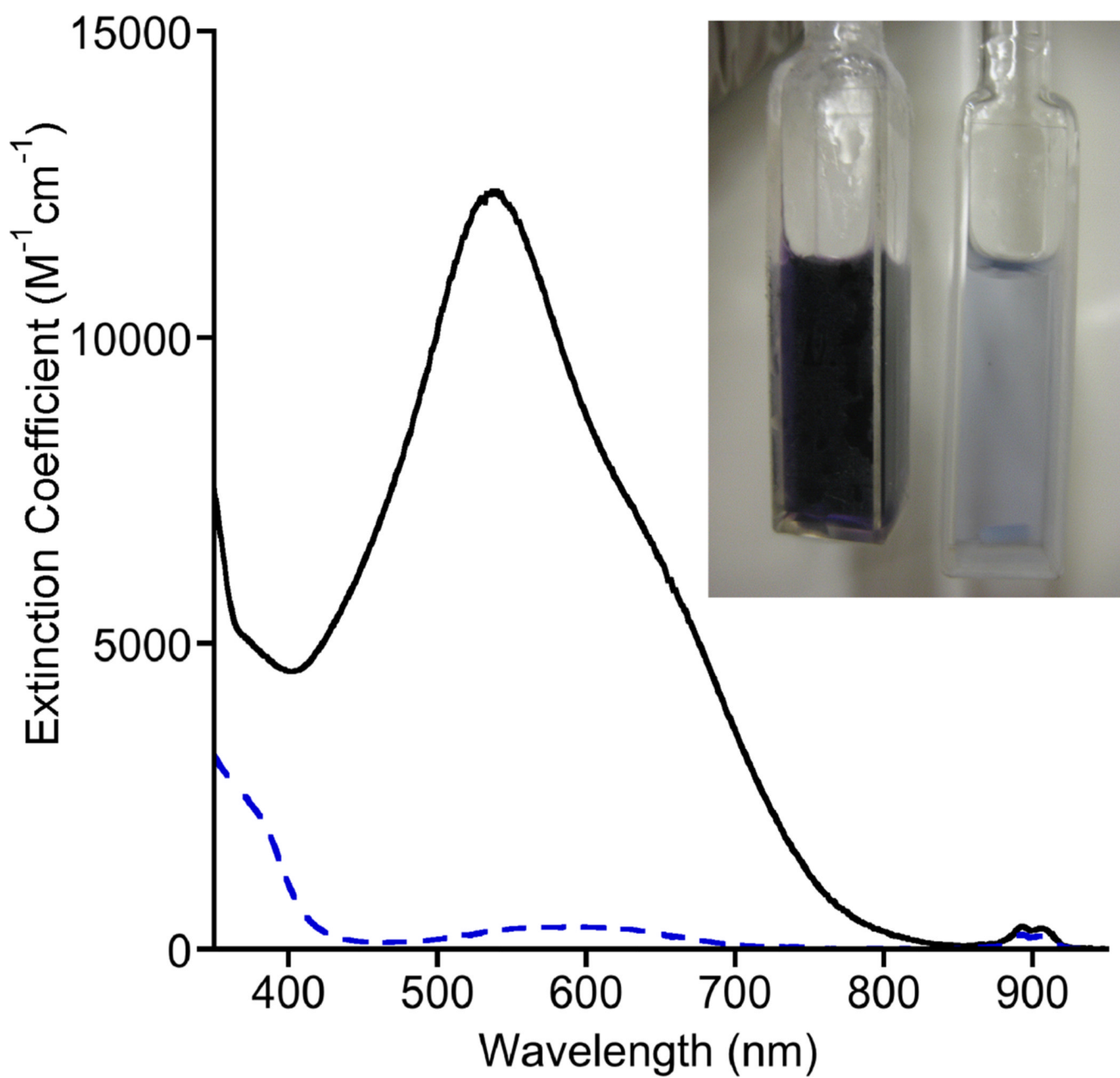


Figure 2. UV-vis spectra of $[Bu_4N][3]$ (blue dashed line, right cuvette in photograph) and **4** (solid black line, left cuvette in photograph) in acetone at $-80\text{ }^\circ\text{C}$.

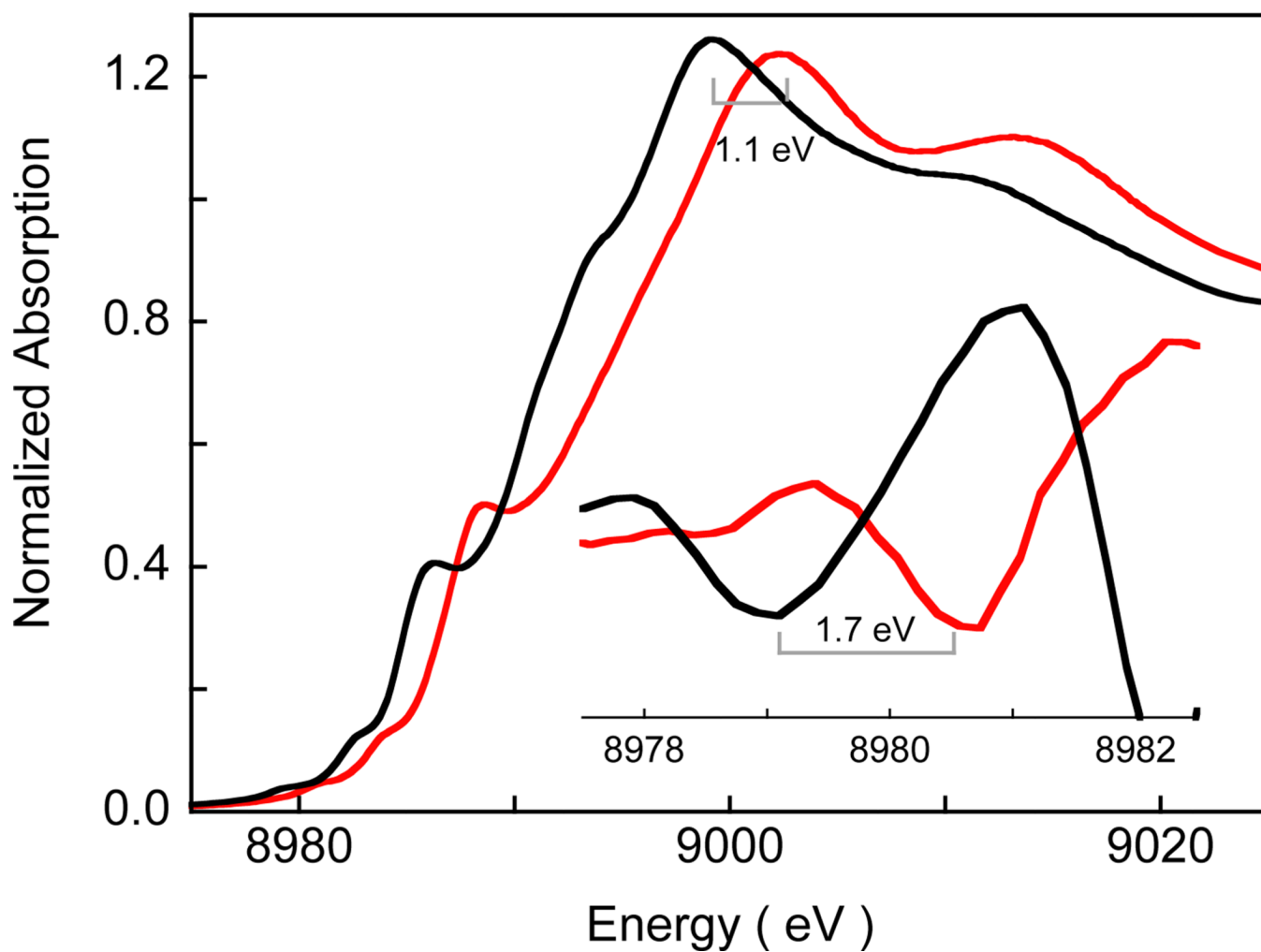


Figure 3. The normalized Cu K-edge XAS spectra of [Bu₄N][3] (—) and 4(—). The inset shows the second derivative spectra of the pre-edge region showing the shift on going from [Bu₄N][3] and 4.

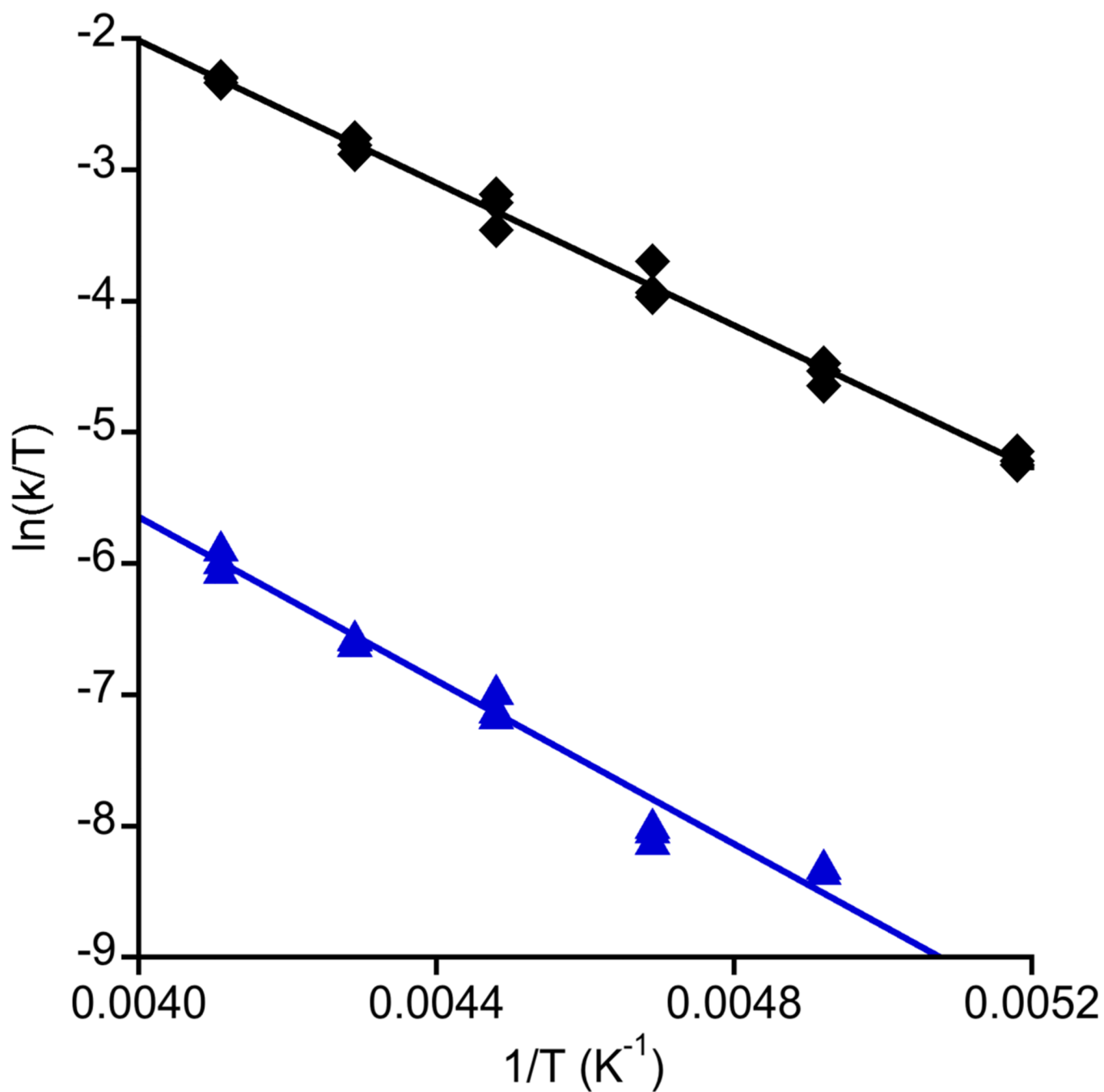


Figure 4. Plots of $\ln(k/T)$ vs. $1/T$ (where k = second order rate constant, T = temperature in K) for the reaction of **4** with DHA (black diamonds) or DHA- d_4 (blue triangles). The shown linear fits were used to calculate the activation parameters listed in the text via the Eyring equation ($R = 0.997$ and 0.985 , respectively).

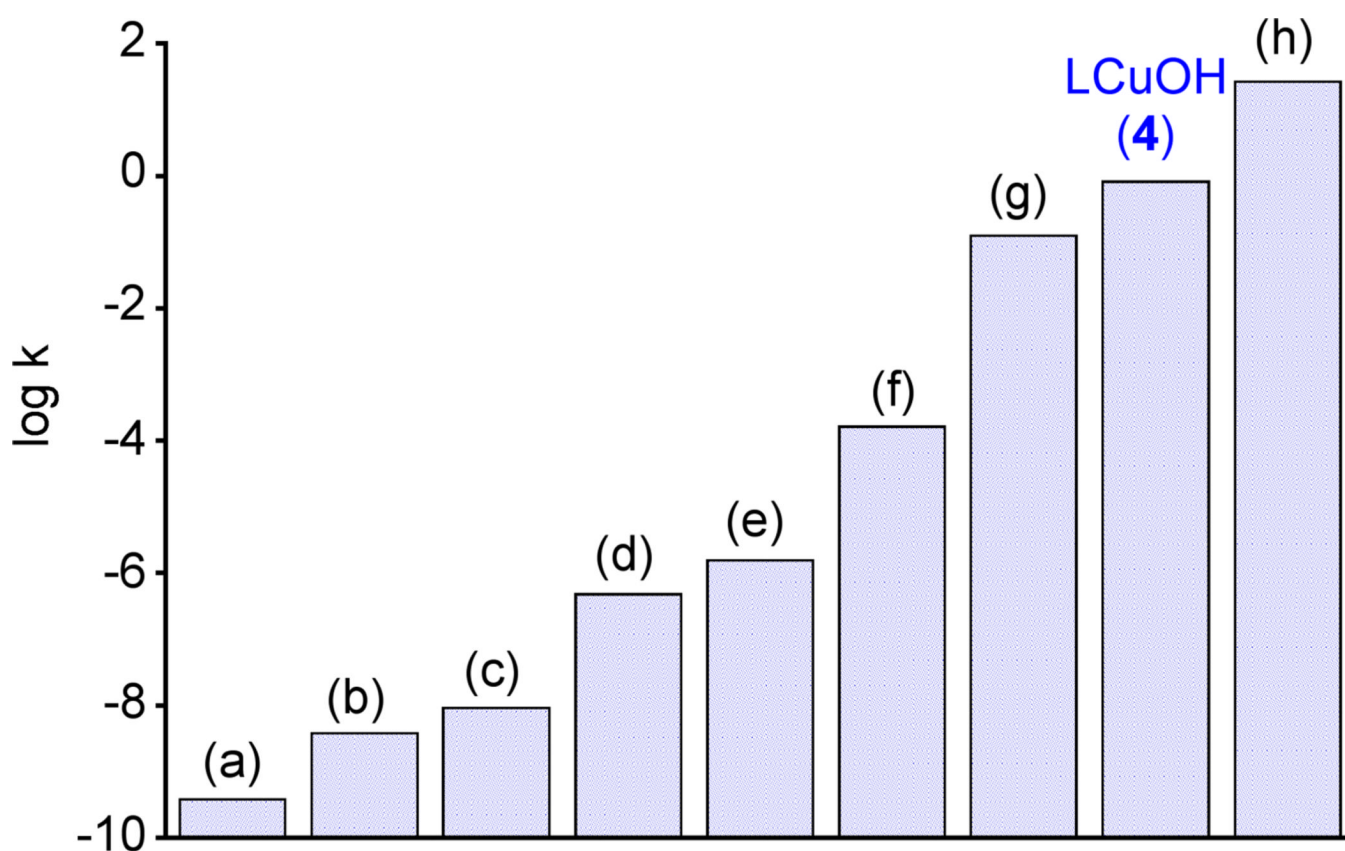


Figure 5.

Comparison of the second order rate constants (k in units of $M^{-1}s^{-1}$, on a logarithmic scale) for oxidation of DHA at $-80\text{ }^{\circ}\text{C}$ by selected copper, iron, and manganese complexes with that of LCuOH (**4**). For (g) and (h), reported rate constants were used; for (a)–(f), the rate constants were calculated using the Eyring equation from the reported activation parameters. (a) $[\text{Cu}^{\text{III}}(\text{Pre})]^+$ (ref. 20) (b) $[\text{Fe}^{\text{III}}(\text{Hbim})(\text{H}_2\text{bim})_2]^{2+}$ (ref. 21), (c) $[\text{Fe}^{\text{III}}(\text{PY5OH})]^{2+}$ (ref. 22), (d) $[\text{Mn}^{\text{III}}(\text{H3buea})\text{O}]^-$, $[\text{MnO}_4]^-$ (refs. 23, 24) (e) $[\text{Mn}^{\text{III}}(\text{PY5OH})]^{2+}$ (ref. 25), (f) $[\text{Mn}^{\text{IV}}(\text{H3buea})\text{O}]^-$, (ref. 23) (g) $[\text{L}'(\text{CH}_3\text{CN})\text{Fe}^{\text{IV}}\text{O}]^{2+}$ (ref. 26), and (h) $[\text{L}'\text{Fe}^{\text{III}}(\text{OH})(\mu\text{-O})(\text{L}')\text{Fe}^{\text{IV}}\text{O}]^{2+}$ (ref. 26). Abbreviations: Pre = 3,9-dimethyl-4,8-diazaundecane-2,10-dionedioximate H_2bim = 2,2'-bi-imidazoline, PY5 = 2,6-bis(bis(2-pyridyl)methoxymethane)pyridine, H3buea $^{3-}$ = triply deprotonated form of tris[(*N'*-*tert*-butylureayl)-*N*-ethylene]amine, L' = tris((4-methoxy-3,5-dimethylpyridin-2-yl)methyl)amine).

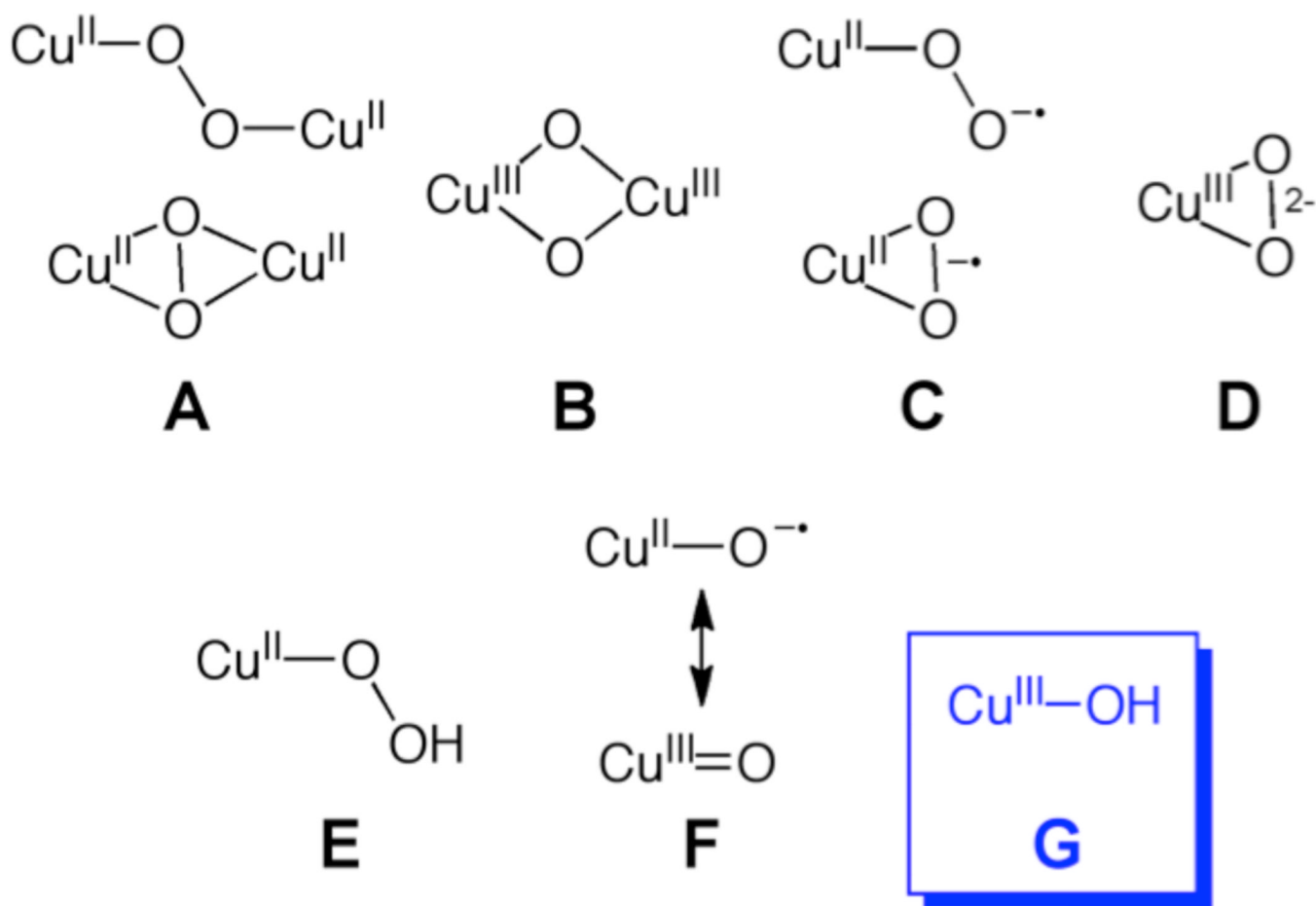


Chart 1.
Copper Oxygen Intermediate Cores.

Table 1Selected Interatomic Distances for 2⁻ and 3⁻ from X-ray Crystallography and *mPW* Calculations^a

	2 ⁻		3 ⁻	
	<i>X-ray</i>	<i>mPW</i>	<i>X-ray</i>	<i>mPW</i>
Cu-N1	1.926(2)	1.961	1.920(2)	1.947
Cu-N2	1.992(2)	2.073	1.996(2)	2.078
Cu-N3	1.993(2)	2.073	2.010(2)	2.080
Cu-X ^b	2.1842(8)	2.216	1.9465(19)	1.863
Cu-N/O (avg)	1.97	2.04	1.97	1.99

^aDistances in Å; X-ray data for PPN⁺ salts.^bFor 2⁻, X = Cl; for 3⁻, X = OH.

Table 2Selected Structural Parameters for 4 from *m*PW Calculations^a

	<i>singlet</i>	<i>triplet</i>
Cu-N1	1.888	1.960
Cu-N2	1.992	2.074
Cu-N3	1.992	2.074
Cu-O	2.155	2.213
Cu-N/O (avg)	1.96	2.04

^aAll distances in Å.